Intrinsic oxidative phosphorylation limitations underlie cellular bioenergetics in leukemia.

Margaret Nelson
East Carolina University
Kelsey McLaughlin
East Carolina University
James Hagen
East Carolina University
Hannah Coalson
East Carolina University
Cameron Schmidt
East Carolina University
Kimberly Kew
East Carolina University
Joseph McClung
East Carolina University
P. Neufer
East Carolina University https://orcid.org/0000-0002-2256-6051
Patricia Brophy
East Carolina University
Nasreen Vohra
East Carolina University
Darla Liles
East Carolina University
Myles Cabot
East Carolina University
Kelsey Fisher-Wellman (fisherwellmank17@ecu.edu)
East Carolina University https://orcid.org/0000-0002-0300-829X

Article

Keywords: leukemia, oxidative metabolism, oxidative phosphorylation

Posted Date: September 2nd, 2020

DOI: https://doi.org/10.21203/rs.3.rs-64203/v1

Abstract

Currently there is great interest in developing cytotoxic pharmacotherapies that disrupt mitochondrial energy transduction in cancer. Given that mitochondria are critical to mammalian energy homeostasis, clinical success of a given therapeutic will undoubtedly hinge upon its cancer cell selectivity. That said, how the mitochondrial network is intrinsically remodeled to drive/enable the cancer phenotype remains a biological black box, largely due to limitations in analytical approaches. Herein, we leveraged an in-house diagnostic biochemical workflow to comprehensively evaluate mitochondrial bioenergetic efficiency and capacity in human leukemia. Using this platform, we provide direct evidence that despite minimal changes in absolute respiratory kinetics, leukemic mitochondria are hallmarked by intrinsic limitations in oxidative phosphorylation (OXPHOS) that constrain the network's ability to contribute to cellular ATP free energy (i.e, ΔGATP) charge. Together, these findings link accelerated oxidative metabolism in leukemia to intrinsic OXPHOS deficiency and provide proof-of-concept that restoring, rather than disrupting, OXPHOS across the leukemic mitochondrial network may represent an untapped, but highly feasible, therapeutic avenue.

Introduction

Although all mitochondria make ATP, the efficiency of this process varies widely across the human body's >200 distinct cell types[1–4]. Tissue-specific differences in mitochondrial function (i.e., mitochondrial specialization) are operationally defined through differences in mitochondrial protein expression, as well as an ever-growing list of post-translational modifications (PTMs)[5–8]. Regardless of the mechanism(s), the biological reward of such specialization is the alignment of bioenergetic efficiency with organ physiology (i.e., establishment of bioenergetic fidelity). In the case of leukemia, as with most cancers, bioenergetic fidelity becomes misaligned from the host, resulting in uncontrolled proliferation of neoplastic progenitors. While this misalignment is in part associated with increased glucose uptake/glycolytic flux, a growing body of evidence is emerging that links multiple aspects of leukemia biology (e.g., tumorigenesis, chemoresistance) to altered mitochondrial quantity and quality[9–14].

In comparison to normal hematopoietic cells, various human leukemias present with increased mitochondrial mass and higher basal respiration rates[10–12,15,16], the latter of which appears to sensitize them to respiratory inhibition[9,13,17,18]. Although these studies have ignited interest in mitochondrial-targeted chemotherapeutics[19,20], experimental rationale for targeting oxidative phosphorylation (OXPHOS) in leukemia is largely based on the assumption that heightened respiration is representative of the cancerous mitochondrial network's attempt to accommodate an increased ATP demand. However, identical increases in mitochondrial respiration can derive from any number of physiological stimuli, ranging from increased demand for ATP resynthesis to decreased OXPHOS efficiency. Distinguishing between these potential outcomes is critical, as such insight demarcates the difference between efficacious targeted drug delivery and undesirable systemic toxicity. For example, it is currently unclear

how targeting 'increased OXPHOS reliance' in leukemia can specifically disrupt leukemic oxidative metabolism without impacting OXPHOS in other highly metabolic organs (e.g., brain, heart, muscle).

Given the ubiquitous necessity of OXPHOS for healthy cellular metabolism, a major barrier to mitochondrial-targeted drugs in leukemia relates to the need for cancer-cell selectivity[21,22]. The current project was based on the premise that establishing cause and effect between mitochondrial bioenergetics and cancer is one of the keys to developing targeted and more effective therapies. To do this requires advanced technical approaches capable of quantifying the interplay among the major mitochondrial thermodynamic free energy driving forces to distinguish between changes in bioenergetic demand versus efficiency. To this end, our group recently developed a diagnostic biochemical workflow that quantifies the changes in free energy driving forces over the entire range of respiratory demand, thus providing a comprehensive profile of mitochondrial bioenergetic efficiency and capacity, relative to the underlying proteome[23–25]. Herein, we leveraged this workflow across several acute leukemia cell lines and primary human leukemias.

Compared to healthy controls, intrinsic limitations to mitochondrial OXPHOS were found to characterize the mitochondrial network in leukemia. Parallel assessment of the underlying mitochondrial proteome linked leukemia-specific OXPHOS deficiency to shifts in adenine nucleotide translocase (ANT) isoform expression and increased abundance of TNF receptor associated protein 1 (TRAP1). Specifically, decreased ANT1 and increased ANT2 in leukemia facilitated matrix ATP uptake, rather than export, that, in the presence of functional TRAP1, directly constrained the ability of mitochondrial OXPHOS to contribute to the cellular ATP free energy (ΔG_{ATP}) charge. These findings are consistent with recent evidence demonstrating that mitochondrial OXPHOS is dispensable for tumor growth[26], and raise the intriguing possibility that the requirement for mitochondria in leukemia may have little to do with oxidative ATP production, but instead reflect a universal requirement for continuous mitochondrial flux to support other cellular functions (e.g., metabolite export, nucleotide synthesis). Taken together, the findings provide proof-of-principle that pharmaceutical intervention designed to restore, rather than disrupt, OXPHOS may impart therapeutic efficacy across various hematological malignancies. Given that increased OXPHOS efficiency is advantageous across non-cancerous tissues, the obvious benefit to this novel treatment paradigm is the elimination of secondary toxicity (i.e., a wide therapeutic window).

Results

Mitochondrial bioenergetic profiling of acute leukemia reveals respiratory flux limitations. To begin to characterize the mitochondrial network in leukemia, we selected three commercially available acute leukemia cell lines – HL-60, KG-1, MV-4-11 – and comprehensively evaluated their bioenergetic profiles. These cells arise from unique precursors along the hematopoietic lineage, express a diverse array of cell surface markers, and have distinct underlying genetics[27–29]. Results were compared to peripheral blood mononuclear cells (PBMC) isolated from healthy volunteers. The utilization of distinct leukemic cell lines,

as well as multiple PBMC controls, was intended to provide the experimental design contrast needed to identify intrinsic mitochondrial bioenergetic signatures potentially necessary for leukemia survival.

Using intact PBMC and leukemia cell lines, respiratory flux (JO_2) was assessed under basal conditions, as well as in response to ATP synthase inhibition (oligomycin), and FCCP titration (i.e., mitochondrial uncoupler). Following FCCP titration, respiration was inhibited with a combination of rotenone (inhibits complex I) and antimycin A (inhibits complex III). Consistent with prior work in human leukemia[10,30], basal respiration normalized to cell count was elevated above PBMC across all leukemia lines and maximal respiratory flux was higher in KG-1 and MV-4-11 (**Fig. 1A**). When normalized to basal respiration, oligomycin similarly inhibited respiration across groups and the fold change induced by FCCP was consistently blunted in leukemia (**Fig. 1B**).

Given the large differences in cell size between PBMC and leukemia (**Supp. Fig. 1A**), we reasoned that normalization to total protein would likely provide the most accurate index of absolute respiratory kinetics across groups. Interestingly, upon normalization to total protein, although basal respiration remained higher in KG-1 and MV-4-11, differences in maximal respiratory flux were eliminated, particularly at higher FCCP concentrations (**Fig. 1C**). In fact, maximal FCCP-supported JO_2 was nearly two-fold lower in HL-60 compared to PBMC when normalized to total protein (**Fig. 1C**). Relative to PBMC, maximal respiration induced by FCCP occurred at much lower concentrations in leukemia (i.e., lower Km; **Fig. 1D**), with increasing FCCP concentrations leading to an overt bioenergetic collapse (i.e., diminishing respiration rates; **Fig. 1C;** compare JO_2 at FC [2.0μM] vs FC [5.0μM]). Similar findings were observed using the mitochondrial uncoupler BAM15 (**Supp. Fig. 1B-C**).

To determine if flux differences in leukemia could be explained by differences in mitochondrial content, nuclear and mitochondrial volumes were assessed independently by tetramethylrhodamine methyl ester (TMRM) or MitoTracker fluorescence and confocal microscopy (**Fig. 1E-I, Supp. Fig 1D**). Absolute nuclear and mitochondrial volumes were higher in all leukemia lines (**Fig. 1E-H**), consistent with leukemia's larger cell size (**Supp. Fig. 1A**). However, when normalized to nuclear volume, mitochondrial content was elevated above PBMC only in HL-60 and MV-4-11 (**Fig. 1I**). Interestingly, across all cell types, considerable discrepancies were apparent when protein-normalized maximal respiratory flux (**Fig. 1C**) was compared to mitochondrial content (**Fig. 1I**). This was particularly evident in HL-60 cells where mean maximal respiration, relative to the size of the underlying mitochondrial network, was ~5-fold lower compared to PBMC (**Fig. 1J**). Together, these data suggested that respiratory flux may be partially constrained across the mitochondrial network in human leukemia, potentially indicative of overt bioenergetic inefficiency.

Intrinsic limitations to OXPHOS kinetics characterize the mitochondrial network in leukemia cell lines. To directly test OXPHOS kinetics in leukemia, two complementary assays were designed, both of which used digitonin-permeabilized cells. In the first assay, the maximal capacity of the electron transport system (ETS) was assessed by energizing permeabilized cells with saturating carbon substrates (Pyr/M/Oct/Glut/Succ; 'MULTI') and titrating in FCCP (**Fig. 2A-B**). The use of multiple substrates was intended to fully saturate the 'fuel' node such that maximal ETS flux could be quantified. Using this

approach, absolute respiration in substrate-replete permeabilized cells was comparable to that observed using intact cells treated with FCCP (**Fig. 2C**), confirming maximal ETS flux in the permeabilized system. Note, maximum FCCP-supported flux under these conditions is indicated throughout as $J\mathrm{H}^{+}_{\mathrm{Total}}$ (**Fig. 2A**). Relative to PBMC and similar to that observed in intact cells, $J\mathrm{H}^{+}_{\mathrm{Total}}$ was lower in HL-60, unchanged in KG-1, and higher in MV-4-11 (**Fig. 2B**).

In mammalian cells, the vast majority of the adenylate pool is represented by ATP (i.e., ΔG_{ATP}), with typical values for ATP free energy ranging from -56 to -64 kJ/mol[31–33]. Thus, to evaluate OXPHOS kinetic efficiency in leukemia mitochondria across a physiological range of ATP resynthesis demands, we utilized the creatine kinase (CK) energetic clamp[23,34,35]. This technique leverages the enzymatic activity of CK, which couples the interconversion of ATP and ADP to that of phosphocreatine (PCr) and free creatine (Cr) such that extramitochondrial ATP free energy (i.e., ΔG_{ATP}) can be empirically titrated using PCr. Using this approach, permeabilized cells were energized with the same carbon substrate mix used for the ETS capacity assay and respiration was stimulated at minimal ATP free energy. Note, ΔG_{ATP} equal to -54.16 kJ/mol reflects an ATP/ADP ratio *in vivo* that would be expected to induce 'maximal' OXPHOS flux and is thus referred to throughout as '$J\mathrm{H}^{+}_{\mathrm{OXPHOS}}$' (**Fig. 2D**). Cytochrome C (Cyt C) was added to assess the integrity of the mitochondrial outer-membrane, and ΔG_{ATP} was then titrated via sequential additions of PCr. With respect to the ETS capacity assay, respiration stimulated by ΔG_{ATP} partially normalized JO_2 between MV-4-11 and PBMC and revealed decreased respiratory kinetics in both HL-60 and KG-1 (**Fig. 2E**), indicating substantial OXPHOS limitations in leukemia.

In both assays, the utilization of identical substrates ('Pyr/M/Oct/Glut/Succ') allowed us to directly quantitate absolute OXPHOS kinetics ('$J\mathrm{H}^{+}_{\mathrm{OXPHOS}}$'), relative to the maximal capacity of the electron transport system, ('$J\mathrm{H}^{+}_{\mathrm{Total}}$'). Together, $J\mathrm{H}^{+}_{\mathrm{OXPHOS}}$ and $J\mathrm{H}^{+}_{\mathrm{Total}}$ provide a quantitative index of fractional OXPHOS capacity as the ratio of the two reflects the proportion of the entire respiratory system that can be used for OXPHOS (**Fig. 2F**). A ratio of '1' reflects maximal OXPHOS reliance, whereas a ratio of '0' indicates that the mitochondrial proton current cannot be utilized for ATP synthesis. Strikingly, calculated fractional OXPHOS in leukemic mitochondria was consistently decreased compared to PBMC, corresponding to a factor of ~0.5 (**Fig. 2G**), indicating that only half of the available ETS capacity in leukemia can be dedicated to OXPHOS under physiological ATP-free energy constraints. Given that the OXPHOS network is responsible for driving ATP/ADP disequilibrium to establish cellular ΔG_{ATP}, low fractional OXPHOS was interpreted to reflect reduced bioenergetic efficiency in leukemia. Moreover, such findings indicate that traditional measurements of 'OXPHOS' capacity using intact cells woefully underestimate true OXPHOS kinetics.

To differentiate between bioenergetic signatures inherent to proliferating cells and those which are unique to leukemia, experiments were repeated in primary human muscle precursor cells (human myoblasts – 'HMB' **Supp. Fig. 2A-B**). These cells were cultured from muscle biopsies uniformly collected from the gastrocnemius muscle (10 cm distal to the tibial tuberosity) of healthy human subjects and were

intended to serve as a non-cancerous human progenitor control. Importantly, fractional OXPHOS was elevated above leukemia in human muscle progenitor cells (**Fig. 2G:** 'HMB'), indicating that decreased bioenergetic efficiency is not an absolute requirement of cellular proliferation, but rather a unique bioenergetic feature of leukemic mitochondria.

Exposure to physiological ΔG_{ATP} reveals direct inhibition of ETS flux by ATP in leukemic mitochondria. To gain insight into the mechanism of OXPHOS limitations in leukemia, at the end of the ΔG_{ATP} titration, oligomycin was added to inhibit ATP synthesis and maximal uncoupled respiration was stimulated with FCCP titration. Maximal FCCP-supported flux under these conditions is denoted as '$FCCP_{\Delta GATP}$' (**Fig. 2D).** In the intact cell assay (**Fig. 1C**), increased glycolytic flux is presumed to maintain cellular ΔG_{ATP} during FCCP titration. Thus, the continued presence of extra-mitochondrial ΔG_{ATP} in our permeabilized cell system was intended to model the adenylate constraints present in intact cells. By comparing maximal OXPHOS flux ('$J{H^+}_{OXPHOS}$') to maximum FCCP-stimulated respiration in the presence of ΔG_{ATP} ('$FCCP_{\Delta GATP}$'), it becomes possible to quantitate any flux limitations imposed by physiological ATP/ADP. Importantly, ATP synthase is not functional during the assay, thus any flux limitations imposed by ΔG_{ATP} would be interpreted to reflect direct ETS regulation. In PBMC and human muscle progenitor cells, the addition of FCCP at the end of the ΔG_{ATP} titration restored respiration to levels obtained under low (-54.16 kJ/mol) ATP free energy (**Fig. 2E, Supp. Fig. 2A-B**), indicating minimal ETS flux inhibition by ΔG_{ATP}. Surprisingly, relative to $J{H^+}_{OXPHOS}$, FCCP-stimulated respiration was substantially blunted in the presence of high ATP free energy across all three leukemia cell lines (**Fig. 2E**), resulting in a 2-fold difference in the $FCCP_{\Delta GATP}/J{H^+}_{OXPHOS}$ ratio, termed 'FCCP Effect' throughout (**Fig. 2H**). Importantly, in the absence of ATP, the addition of CK and PCr up to 21mM did not impact FCCP-supported flux in permeabilized MV-4-11 cells (**Supp. Fig. 2C**), confirming that ATP free energy was required to induce ETS flux inhibition in leukemia. To determine the sensitivity of ETS inhibition by ΔG_{ATP}, FCCP-supported flux in MV-4-11 cells was assessed at defined ATP free energies. In these experiments, extramitochondrial ΔG_{ATP} was administered after CV inhibition with oligomycin, followed by FCCP titration. Results revealed a dose-dependent decrease in uncoupled respiration in response to increasing ΔG_{ATP} (**Fig. 3A**).

Inhibition of respiratory flux mediated by ΔG_{ATP} could reflect a number of potential mechanisms ranging from cytoskeletal alterations, direct inhibition of the matrix dehydrogenase network (e.g., inhibitory phosphorylation of pyruvate dehydrogenase), and/or ETS inhibition[23]. To differentiate between these potential outcomes, mitochondria were isolated from PBMC and each of the three leukemia cell lines and similarly assessed for OXPHOS kinetics. In mitochondria energized with saturating carbon, increasing ΔG_{ATP} led to a more pronounced decrease in respiration in mitochondria of all three leukemia cell lines. The ability of FCCP to restore maximal respiratory flux was also once again blunted in leukemia mitochondria (**Fig. 3B-C**), consistent with lower fractional OXPHOS (**Fig 2G**). This inhibitory effect of ATP free energy on $J{H^+}_{Total}$ was present in both isolated leukemia cell mitochondria and permeabilized leukemia cells, ruling out any involvement of the cytoskeleton. Together these findings demonstrate that

mitochondrial flux inhibition by ATP free energy is an intrinsic bioenergetic feature of leukemic mitochondria.

To differentiate between respiratory flux inhibition localized to the matrix dehydrogenases or the ETS, NADH/NAD^+ redox poise was measured in parallel in substrate-replete isolated mitochondria exposed to an identical ΔG_{ATP} span. Results are depicted as a percentage of complete reduction, where 0% reduction reflects isolated mitochondria at 37°C without added substrates and 100% reduction is recorded at the end of the assay with the addition of cyanide. Except for a slight hyper-reduction in HL-60 mitochondria, NADH/NAD^+ redox was similar across groups (**Supp. Fig. 2D**), indicating that ATP-mediated respiratory flux inhibition in leukemia is not due to a generalized impairment in dehydrogenase flux. Having eliminated the cytoskeleton and the dehydrogenase network as potential sites of inhibition, we next turned our attention to the ETS. To determine if flux inhibition induced by ΔG_{ATP} was specific to a given respiratory complex, OXPHOS kinetics was assessed in isolated mitochondria energized with either complex I (CI)- or CII-linked substrate combinations. Note, the presence of saturating malate in the CI substrate mix results in CII inhibition via malate-fumarate equilibration (**Fig. 3D**). Likewise, the addition of rotenone in the presence of succinate eliminates residual CI-supported flux by downstream products of succinate oxidation (**Fig. 3D**). Using either CI- or CII-linked substrates, we once again observed a more pronounced decrease in respiration in response to ΔG_{ATP} titration in leukemia mitochondria, as well as a stark inability of FCCP to restore maximal respiratory flux (**Fig. 3E-H**). Taken together, these findings indicate that ΔG_{ATP}-mediated respiratory flux limitations are specific to leukemia mitochondria, independent of carbon substrate source, and thus most likely attributable to ETS inhibition, potentially downstream of CI or CII.

Subcellular proteomics reveals unique isoform expression of the adenine nucleotide translocase (ANT) in leukemia. To identify potential protein mediators responsible for reduced bioenergetic efficiency in leukemia, we conducted a proteomics screen using TMT-labeled peptides prepared from the same isolated mitochondria samples used for functional characterization. To control for group differences in percent mitochondrial enrichment, nLC-MS/MS raw data were searched using the MitoCarta 2.0 database, as previously described[36]. Using this approach, total mitochondrial protein abundance was similar between groups (**Supp. Table 1**), thus allowing for intrinsic mitochondrial signatures to be identified across leukemia. In total, 135 differentially expressed mitochondrial proteins (adjusted P value < 0.01) were identified comparing PBMC to each of the three leukemia lines (**Fig. 4A**). For pair-wise comparisons of mitochondrial protein expression between PBMC and each of the three leukemia cell lines, see **Supp. Table 1**. With respect to the shared differentially expressed proteins, several of these proteins have previously been implicated in cancer biology, such as decreased MAOB[37] and HK1[38], and increased MTHFD1L[39], and COX17[40] (**Fig. 4A**).

Focusing on the OXPHOS proteome, we assessed the abundance of the individual protein subunits that comprise CI, CII, CIII, and CIV, as well as the protein components of the phosphorylation system which include ATP synthase (CV), the phosphate carrier (SLC25A3), and ANT (**Fig. 4B**). Although considerable

heterogeneity was present across groups, comparing protein expression profiles of the individual subunits that comprise CI-CV and SLC25A3 (**Fig. 4C**, **Supp. Fig. 3A-D**) revealed that only 6 of the 110 subunits were similarly altered in leukemia (**Supp. Table 1**). With the exception of COX6A1, all protein subunits were involved in the assembly of CI (NDUFB10), CIV (COA4, COA7, COX17) or CV (ATPAF2). In stark contrast, the expression profiles of the three main ANT isoforms were entirely distinct between PBMC and leukemia mitochondria, highlighted by reduced ANT1 (SLC25A4) and increased ANT2 (SLC25A5) and ANT3 (SLC25A6) in leukemia (**Fig. 4D**).

Inhibition of ETS flux by ΔG_{ATP} requires ANT. Given that ATP free energy was required to induce ETS flux inhibition, we hypothesized that this effect may be mediated by ATP transport into the matrix, facilitated by enhanced ANT2 expression in leukemia[41]. To test this hypothesis, FCCP-supported respiration was assessed in energized, permeabilized MV-4-11 and HL-60 cells exposed to ΔG_{ATP} of -61.49 kJ/mol in the absence and presence of the ANT inhibitor carboxyatractyloside (CAT)[42]. Consistent with our prior findings, the addition of FCCP in the presence of ΔG_{ATP} was incapable of restoring flux to levels obtained with minimal ATP free energy in leukemia (**Fig. 5A-B**; 'ΔG_{ATP} (-61.49 kJ/mol)'). However, relative to no adenylates, as well as minimal ΔG_{ATP} (e.g., - 54.16 kJ/mol), the addition of CAT restored maximal FCCP-supported ETS flux in the presence of high ATP free energy (**Fig. 5A-C**). Similar experiments performed in MV-4-11 isolated mitochondria (**Fig. 5D**), as well as with the ANT inhibitor bongkrekic acid (**Supp. Fig. 4C**) revealed nearly identical results, confirming that ETS flux inhibition by ΔG_{ATP} requires functional ANT. Together, these findings reveal an intrinsic bioenergetic phenotype, specific to leukemia, whereby extramitochondrial ATP gains access to the matrix space, presumably via increased ANT2, and directly constrains ETS flux across a physiological ΔG_{ATP} span.

Reduced mitochondrial bioenergetic efficiency is a common feature of human leukemia. To determine if the bioenergetic phenotypes present in leukemia cell lines translated to the clinic, we recruited patients diagnosed with leukemia and comprehensively evaluated mitochondrial bioenergetic function in mononuclear cells isolated from bone marrow aspirates. Although all patients had confirmed leukemia at the time of sample acquisition, the type of leukemia ranged from acute myeloid leukemia (N=5), chronic myeloid leukemia (CML, N=2), and granular lymphocytic leukemia (N=1). Biochemical results were compared to PBMC isolated from age-matched participants without a prior history of leukemia. Mitochondrial respiration rates in substrate-replete permeabilized cells in the absence of adenylates were identical between groups (**Fig. 6A**). In contrast, respiration stimulated by ΔG_{ATP} revealed decreased OXPHOS kinetics in primary leukemic cells (**Fig. 6B**). In agreement with impaired OXPHOS flux in leukemia, calculated fractional OXPHOS was reduced in primary leukemia (**Fig. 6C**), entirely consistent with results observed across the leukemia cell lines (**Fig. 2G**). To determine if ΔG_{ATP} was capable of directly limiting ETS flux via ANT-mediated ATP uptake, FCCP titration was performed using substrate-replete permeabilized cells in the absence (**Fig. 6B**) and presence (**Fig. 6D**) of carboxyatractyloside. In the absence of ANT inhibition, the presence of ΔG_{ATP} restricted FCCP-supported flux specifically in leukemic cells (**Fig. 6B**, quantified in **Fig 6E**; '- CAT'). Despite the continued presence of ΔG_{ATP}, the addition of CAT

restored FCCP-supported flux in leukemic cells to that of PBMC (**Fig. 6D**, quantified in **Fig 6E**), confirming direct ETS flux inhibition by ATP in primary leukemia. Taken together, these findings from primary human leukemia cells corroborate the results across the three acute leukemia cell lines and suggest that specific impairments in OXPHOS kinetics is a hallmark characteristic of the mitochondrial network in human leukemia.

Inhibition of ETS flux via extramitochondrial ΔG_{ATP} requires functional TRAP1. Having established that extramitochondrial ΔG_{ATP} must gain access to the matrix space to inhibit ETS flux in leukemia, we next set out to elucidate the potential protein mediator(s) of this effect. To do this, we searched our proteomics dataset for mitochondrial proteins with known kinase and/or ATPase function that were substantially upregulated across all three leukemia lines and identified mitochondrial TRAP1 (**Fig. 7A**). TRAP1 is the mitochondrial paralog of the heat shock protein 90 (HSP90) family and is widely recognized as a potential anti-cancer drug target across multiple human malignancies, including leukemia[43–49]. Given that ATPase activity is required for TRAP1 function[50], we hypothesized that ETS inhibition in leukemic mitochondria exposed to ΔG_{ATP} may be driven by acute activation of TRAP1. To test this hypothesis, OXPHOS kinetics were assessed in permeabilized MV-4-11 cells in the absence and presence of the TRAP1 inhibitor 17-AAG[51]. In substrate-replete permeabilized MV-4-11 cells, the presence of 17-AAG had no impact on maximal FCCP-supported respiration (**Supp. Fig. 4A**), indicating that TRAP1 does not impinge on ETS flux in the absence of physiological adenylates. Remarkably, the presence of 17-AAG increased $J{H^+}_{OXPHOS}$ and calculated fractional OXPHOS relative to vehicle control and completely restored FCCP-supported respiration in the presence of ATP free energy (**Fig. 7B-D**). Similar results were observed using permeabilized HL-60 cells (**Supp. Fig. 4B, Fig. 7C-D**), as well as using the mitochondrial-targeted TRAP1 inhibitor Gamitrinib TPP hexafluorophosphate (**Supp. Fig. 4C**).

Given that functional TRAP1 was apparently required for ATP-mediated respiratory inhibition in leukemia, we next sought to determine the sensitivity of TRAP1 to physiological ΔG_{ATP}. Related to this, although ATP is widely understood to be the universal energy currency in cells, it is critical to consider that ATP alone has minimal bio-synthetic power; rather, its utilization as a common energy currency is solely a function of the remarkable displacement of the molecule from equilibrium (~10 orders of magnitude)[52]. This means that biological processes driven by ATP hydrolysis, such as those carried out by TRAP1, are presumably fueled by ATP free energy, rather than ATP levels per se. The primary advantage of the CK clamp technique is that it allows for mitochondrial bioenergetics to be evaluated across a physiological ΔG_{ATP} span without appreciable changes in ATP concentration (**Supp. Fig. 4D**). Thus, we reasoned that the CK clamp could be utilized to assess TRAP1 sensitivity to ΔG_{ATP} under conditions in which free [ATP] is not rate-limiting. To do this, we assessed the ability of 17-AAG to impact FCCP-supported respiration across a physiological ΔG_{ATP} span. For contrast, we compared the respiratory impact of 17-AAG to that of the commonly used ETC inhibitor antimycin A. Although antimycin A decreased respiratory flux in permeabilized MV-4-11 cells, percent inhibition by the compound was largely insensitive to ΔG_{ATP}, consistent with direct respiratory complex inhibition (**Supp. Fig. 4E**). In contrast, across all leukemia cell

lines, respiratory inhibition induced by functional TRAP1 was exquisitely sensitive to ΔG_{ATP} (**Fig. 7E-G**), indicating that the ability of TRAP1 to impinge on ETS flux depends entirely upon the prevailing matrix ATP free energy. Given that we observed similar maximal respiratory capacities using both intact and permeabilized cells (**Fig. 2C**), these data inform a model whereby intrinsic OXPHOS limitations in leukemia serve to chronically constrain the mitochondria's ability to drive ATP/ADP disequilibrium, thereby lowering cellular ΔG_{ATP} charge and stimulating compensatory rapid and continuous metabolic flux (**Fig. 7H**).

Discussion

Increased mitochondrial oxidative metabolism, an established metabolic hallmark of leukemia[10,11,13,17,53,54], has been historically interpreted to reflect an increased reliance on mitochondrial ATP production. However, direct evaluation of fractional OXPHOS kinetics had not been empirically evaluated in leukemia at the onset of this project. Thus, it remained to be determined whether higher basal respiration in leukemia reflected accelerated demand for ATP regeneration or intrinsic bioenergetic inefficiency. Both conditions would be expected to similarly restrict cellular ATP/ADP equilibrium displacement (i.e., ΔG_{ATP} charge) and thus potentially result in identical respiratory profiles in intact cells. Applying a diagnostic biochemical workflow, we determined that intrinsic limitations in fractional OXPHOS characterize the mitochondrial network across human leukemias. In fact, approximately half of the leukemic mitochondrial network is incapable of contributing to oxidative ATP production across a physiological ΔG_{ATP} span. Subsequent experiments linked intrinsic OXPHOS limitations in leukemia to a unique biochemical mechanism in which extra-mitochondrial ATP gained access to the matrix space, where it then directly inhibited electron transport flux in a ΔG_{ATP}-dependent manner. Restoration of mitochondrial bioenergetic efficiency was observed upon administration of 17-AAG, unveiling a critical role for the pro-neoplastic protein TRAP1 in driving reduced fractional OXPHOS in leukemia.

Although prior work has implicated ANT2[42,55,56] and TRAP1[50] as potential anti-cancer targets in leukemia, we present for the first time here a potential mechanism for their coordinated regulation of leukemic cell metabolism. Specifically, our findings inform a model of leukemia bioenergetics in which decreased ANT1 and increased ANT2 favors the uptake of extra-mitochondrial ATP into the matrix space. The transfer of ΔG_{ATP} from the cytosol to the matrix in turn activates matrix-localized TRAP1 by providing substrate for its ATPase activity. While TRAP1 has been shown to interact with CII and CIV of the ETS[48], the present findings challenge the conclusion that activated TRAP1 directly inhibits ETS flux as a means of upregulating glycolytic metabolism. In fact, the exquisite sensitivity of TRAP1 to ΔG_{ATP} *in vitro* indicates that TRAP1 restricts the ability of the mitochondrial network to contribute to the cellular ΔG_{ATP} charge. In this way, chronic maintenance of low ΔG_{ATP} maximizes both glycolytic and mitochondrial metabolism, entirely consistent with the known metabolic phenotype of human leukemia[11,12,15]. Such conditions are likely advantageous to proliferating leukemic blasts, as the increased ATP demand commensurate with pro-growth signaling[57,58] likely synergizes with OXPHOS limitations to chronically

constrain cellular ΔG_{ATP}, thereby establishing the thermodynamic metabolic 'pull' needed for rapid and continuous nutrient flow across the plasma membrane (**Fig. 7H**). Although ΔG_{ATP} in proliferating blasts was not directly quantified here, the ATP free energy-dependent ETS inhibition by TRAP1 (**Fig. 7E-G**) strongly suggests a low (i.e., more positive) ΔG_{ATP} is maintained in leukemia.

Currently, there is great interest in developing novel pharmacotherapies that target mitochondrial OXPHOS in leukemia[13,16,17,19,20]. Yet, a large caveat of targeting mitochondria is the ubiquitous necessity of OXPHOS for healthy cellular metabolism. If indeed the proliferative potential of leukemia depends upon maintenance of low fractional OXPHOS, it is tempting to speculate that a pharmaceutical intervention designed to restore normal ΔG_{ATP} could effectively halt cell proliferation, in turn allowing for these blasts to succumb to apoptosis. Such a targeted approach would minimize secondary toxicity as increased OXPHOS efficiency is advantageous across non-cancerous, highly metabolic tissues (e.g., brain, heart, muscle), as well as in the context of adaptive cellular immunity[59,60]. Based upon our proposed model, targeting the acute ETS regulating capabilities of the pro-neoplastic protein, TRAP1, provides an appealing, leukemia specific target for pharmaceutical intervention, as acute TRAP1 inhibition in the matrix restored OXPHOS kinetics in leukemic mitochondria. Moreover, given that TRAP1 has previously been shown to interact with matrix localized c-Src[47], it is possible that TRAP1 activation indirectly regulates respiratory flux in leukemia by facilitating post-translation OXPHOS inhibition (i.e., inhibitory phosphorylation).

Taken together, the present findings provide a novel mechanism to explain the enhanced glycolytic flux and altered mitochondrial metabolism previously observed in leukemia[1,2,5–7]. In particular, we provide direct evidence that leukemic blasts display an inherent limitation in OXPHOS kinetics that is mediated by a dynamic interplay between TRAP1 ATPase activity and the cellular ATP free energy. Lastly, this study establishes the utility of comprehensive mitochondrial diagnostics to inform therapeutic strategies targeting OXPHOS in leukemia and sets the stage for an entirely new research area focused on understanding and leveraging the unique biochemical characteristics intrinsic to cancerous mitochondria.

Methods

Unless otherwise stated, all reagents and chemicals were purchased from Sigma-Aldrich.

Blood collection and isolation of PBMCs

All procedures involving human subjects were approved by the Institutional Review Board of the Brody School of Medicine. Venous blood from the brachial region of the upper arm was collected from 30 healthy volunteers, ranging from 18-70 years. Whole blood was collected in 20 sodium-heparinized Cell Preparation Tubes (CPT) (BD Biosciences, Franklin Lakes, NJ) and centrifuged at 1,800 x g for 15 min. Fractions containing peripheral blood mononuclear cells (PBMC) were collected from 4 CPT tubes and used for intact and permeabilized cell experiments while the remaining PBMC fractions were used to isolate mitochondria.

Mononuclear cell isolation from bone marrow aspirates

Bone marrow aspirates were collected from patients undergoing confirmatory diagnosis for a range of hematological malignancies. Patients with confirmed leukemia were enrolled in the study. Type of leukemia ranged from acute myeloid leukemia (AML, N=5), chronic myeloid leukemia (CML, N=2), and granular lymphocytic leukemia. Patient age ranged from 32-78 years (male/female, 3/5). Bone marrow aspirates were compared to PBMC isolated from age-matched participants without a prior history of any hematological malignancy. Peripheral blood and bone marrow aspirates were collected in sodium-heparinized Cell Preparation Tubes (CPT) (BD Biosciences, Franklin Lakes, NJ) and centrifuged at 1,800 x g for 15 min. Mononuclear cells were isolated and then washed in ammonium-chloride-potassium (ACK) lysis buffer to remove red blood cells.

Cell culture

HL-60, KG-1, and MV-4-11 (ATCC, Manassas, VA) human leukemia cells were cultured in IMDM (Thermo Fisher Scientific, Waltham, MA) supplemented with glutamine, 10% FBS, and 1% penicillin/streptomycin and incubated at 37°C in 5% CO_2. Upon reaching an average cell density of $1.5x10^6$cell/mL the cells were harvested and used for whole cell and isolated mitochondria experiments. Primary human muscle progenitor cells (human myoblasts, 'HMB') were derived from fresh muscle biopsy samples, as described previously[61]. Cells were cultured on collagen-coated flasks using HMB growth medium (GM: Ham's F10, supplemented with 20% FBS and 1% penicillin/streptomycin, and supplemented immediately prior to use with 5 ng/ml basic FGF).

Confocal Microscopy

Cells were pre-loaded with 200nM Mitotracker Green-FM dye (MTG-FM; Molecular Probes, Eugene, OR) at 37°C for 1hr. Cells were then centrifuged at 300 x g for 7min at ~25°C and resuspended in MTG-FM-free IMDM formulation media (Thermo Fisher) containing 50nM tetramethyl rhodamine methyl ester (TMRM) and 2μM Hoechst 33342. Cells were plated on glass-bottom dishes (MatTek, Ashland, MA) for imaging. Cells were held in place with a thin 1% agarose pad that was applied immediately prior to imaging in order to minimize rapid motion interference during imaging of live non-adherent cells[62].

All imaging was performed using an Olympus FV1000 laser scanning confocal microscope (LSCM) with an onstage incubator at 37°C. Acquisition software was Olympus FluoView FSW (V4.2). The objective used was 60X oil immersion (NA=1.35, Olympus Plan Apochromat UPLSAPO60X(F)). Images were 800x800 pixel with 2μs/pixel dwell time, sequential scan mode, resulting in a 4X digital zoom. Hoechst 33342 was excited using the 405nm line of a multiline argon laser; emission was filtered using a 560nm dichroic mirror and 420-460nm barrier filter. MTG-FM was excited using the 488nm line of a multiline argon laser; emission was filtered using a 560nm dichroic mirror and 505-540nm barrier filter. TMRM was excited using a 559nm laser diode; emission was filtered using a 575-675nm barrier filter. Zero detector offset was used for all images and gain at the detectors was kept the same for all imaging. The pinhole aperture diameter was set to 105μm (1 Airy disc).

Images were analyzed using Fiji[63]. Spatial resolution was measured using sub-resolution fluorescent beads (Thermo Fisher) and curve fitting was performed using the MetroloJ plugin in Fiji. 16-bit images were made into a composite. Circular ROIs were manually selected using the ROI manager plugin. Images were then decomposed into separate 16-bit image stacks leaving the ROI positions intact. A Huang auto-threshold was used for automated selection of signal for all three channels. Following threshold application, each signal was measured using the multi-measure feature. Only whole cells were analyzed (i.e. cells on edges of the FOV were excluded). Slices containing cells above the lowest monolayer were removed from stacks to avoid oversampling. The following calculations were performed to determine the relevant signal volumes.

Signal Volume (μm^3) = [A*Z]/N

Where A is the signal-positive area selected using a Huang auto-threshold (μm^2), Z is the optical section thickness (axial resolution; μm), and N is the number of steps within each optical section (i.e. axial resolution divided by the step size). The latter operation is necessary to correct for oversampling of the signal volumes.

Respiratory flux in intact and permeabilized cells

Approximately 3 x 10^6 cells were used for each intact and permeabilized cell experiment. High-resolution respirometry measurements were performed using the Oroboros Oxgraph-2k (O2k; Oroboros Instruments, Innsbruck, Austria) in a 1mL reaction volume at 37°C. At the conclusion of each experiment 1mL of cell suspension was collected from each chamber and centrifuged at 2,000 x g for 10 min at 4°C. Cells were lysed using low-percentage detergent buffer (CelLytic) followed by a freeze-thaw cycle, and protein concentration was determined using a BCA protein assay.

Respiratory flux was measured using previously described methods[23]. For intact cell measurements, PBMC and leukemia cells were resuspended in Intact Cell Respiratory Media (17.7g/L Iscove's Modified Dulbecco's Medium (IMDM), 20mM HEPES, 1% Penicillin/Streptomycin, 10% FBS, pH 7.4). After basal respiration was established, oligomycin (Oligo; 0.02μM) was added followed by FCCP titration (FC; 0.5-5μM), rotenone (Rot; 0.5μM) and antimycin A (Ant; 0.5μM). For permeabilized cell measurements, PBMC and leukemia cells were resuspended in Respiratory Buffer supplemented with creatine (105mM MES potassium salt, 30mM KCl, 8mM NaCl, 1mM EGTA, 10mM KH_2PO_4, 5mM $MgCl_2$, 0.25% BSA, 5mM creatine monohydrate, pH 7.2). Cells were permeabilized with digitonin (Digi; 0.02mg/mL), and respiratory flux was measured using the creatine kinase (CK) clamp and FCCP titration assays. Within the CK clamp assay, the free energy of ATP hydrolysis (ΔG_{ATP}) is calculated using the equilibrium constant for the CK reaction (K'_{CK}) and is based upon the addition of known concentrations of creatine (Cr), phosphocreatine (PCr), and ATP in the presence of excess amounts of CK[23]. Calculation of ΔG_{ATP} at defines PCr concentrations was done using the online resource (https://dmpio.github.io/bioenergetic-calculators/ck_clamp/) previously described[23].

For all assays, various combinations of carbon substrates and inhibitors were employed. Substrates and inhibitors utilized are indicated in the figure legends: CK (20U/mL), ATP (5mM), PCr (1mM, 6mM, 15mM, 21mM), pyruvate (5mM), malate (1mM), glutamate (5mM), octanoyl-carnitine (0.2mM), succinate (5mM) cytochrome C (Cyt C, 10µM), oligomycin (Oligo, 0.02µM), FCCP (FC, 0.5-2µM), rotenone (Rot, 0.5µM), antimycin A (Ant A, 0.5µM), carboxyatractyloside (CAT, 1µM), bongkrekic acid (20µM), 17-AAG (sigma, #100068, 1µM), Gamitrinib TPP hexafluorophosphate (MedChemExpress, #HY-102007A, 1µM).

Isolation of mitochondria from PBMCs and leukemia cells

In order to pellet cells, PBMC fractions were washed with PBS and centrifuged at 3,000 x g for 10 min at 4°C and leukemia cells were centrifuged at 300 x g for 10 min followed by a PBS wash. Cell pellets were resuspended in Mitochondrial Isolation Buffer with BSA (100mM KCl, 50mM MOPS, 1mM EGTA, 5mM $MgSO_4$, 0.2% BSA, pH 7.1) and homogenized using a borosilicate glass mortar and Teflon pestle. Homogenates were centrifuged at 800 x g for 10 min at 4°C. The supernatant was collected, and the remaining pellet was resuspended in Mitochondrial Isolation Buffer with BSA, then homogenized and centrifuged again. This process was repeated a total of 3 times. The collected supernatant was centrifuged at 10,000 x g for 10 min at 4°C to pellet the mitochondrial fraction. The fraction was resuspended in Mitochondrial Isolation Buffer without BSA, transferred to a microcentrifuge tube and subjected to a second spin at 10,000 x g. The mitochondrial pellet was resuspended in ~100µL of Mitochondria Isolation Buffer and protein concentration was calculated using the Pierce BCA assay. Respiration assays using isolated mitochondria were similar to that described for permeabilized cells.

Mitochondrial NADH/NAD^+ redox in isolated mitochondria

Fluorescent determination of NADH/NAD^+ was performed using a QuantaMaster Spectrofluorometer (QM-400, Horiba Scientific, Kyoto, Japan). The NADH/NAD+ was detected at Ex/Em: 350/450. NADH/NAD+ was measured in mitochondria isolated from PBMC and leukemia cell lines using the CK clamp assay. Experiments were performed at 37°C in a 200µL reaction volume. To start, Respiratory Buffer supplemented with creatine (200µL), Cyt C (10µM), mitochondrial lysate (100µg) were added into a glass cuvette. Mitochondria were incubated at 37°C for ~ 5 minutes in the absence of substrate to induce 0% reduction of the NADH pool. Saturating carbon substrates were added (Pyr/Mal/ Oct/Glut/Succ, 'Multi'), and respiration was stimulated with the CK clamp. Titration of ΔG_{ATP} was performed via PCr titration (6, 15, 21mM). Oligomycin (0.02µM) was added to inhibit ATP synthesis and cyanide (CN, 10mM) was added to induce 100% reduction of the matrix NADH pool. The NADH/NAD+ was expressed as a percentage reduction of the CN value (i.e. 100% reduction) based upon the formula % Reduction = $(F-F_{0\%})/(F_{100\%}-F_{0\%})*100$.

Mitochondrial lysis, protein digestion, and peptide labeling for TMT quantitative proteomics

Mitochondrial pellets from leukemia cells and PBMC (approximately 250 µg of protein) were lysed in ice-cold 8 M Urea Lysis Buffer (8 M urea in 50 mM Tris, pH 8.0, 40 mM NaCl, 2 mM $CaCl_2$, 1x cOmplete ULTRA mini EDTA-free protease inhibitor tablet), as described previously[36]. The samples were frozen on dry ice and thawed for three freeze-thaw cycles and further disrupted by sonication with a probe sonicator in three 5s bursts set at an amplitude of 30 (Q Sonica, Newtown, CT). Samples were centrifuged at 10,000 × g for 10 min at 4 °C to pellet insoluble material. Protein concentration was determined by BCA, and equal amounts of protein (200 µg, adjusted to 2.5 mg/mL with Urea Lysis Buffer) were reduced with 5 mM DTT at 32 °C for 30 min, cooled to room temperature, and then alkylated with 15 mM iodoacetamide for 30 min in the dark. Unreacted iodoacetamide was quenched by the addition of DTT up to 15 mM. Initial digestion was performed with Lys C (Thermo Fisher) 1:100 w-w; 2 µg enzyme per 200 µg protein) for 4 hr at 32 °C. Following dilution to 1.5 M urea with 50 mM Tris (pH 8.0), 30 mM NaCl, 5 mM $CaCl_2$, the samples were digested overnight with trypsin (Promega, Madison, WI) 50:1 w/w, protein:enzyme at 32 °C. Samples were acidified to 0.5% TFA and centrifuged at 10,000 × g for 10 min at 4 °C to pellet insoluble material. Supernatant containing soluble peptides was desalted on a 50 mg tC18 SEP-PAK solid phase extraction column (Waters, Milford, MA) and eluted (500 µL 25% acetonitrile/0.1% TFA and 2 × 500 µL 50% acetonitrile/0.1% TFA). The 1.5 mL eluate was frozen and lyophilized.

TMT labeling

TMT labeling was performed as previously described[36]. The samples from isolated mitochondria were re-suspended in 100 µL of 200 mM triethylammonium bicarbonate (TEAB), mixed with a unique 10-plex Tandem Mass Tag (TMT) reagent (0.8 mg re-suspended in 50 µL100% acetonitrile), and shaken for 4 hr at room temperature (Thermo Fisher). A total of 2 x 10-plex kits were used and one sample was TMT-labeled in both kits to control for quantification differences across multiplex preparations. Following quenching with 0.8 µL 50% hydroxylamine samples were frozen, and lyophilized. Samples were re-suspended in ~1 mL of 0.5% TFA and again subjected to solid phase extraction, but with a 100 mg tC18 SEP-PAK SPE column (Waters). The multiplexed peptide sample was subjected to high pH reversed phase fractionation according to the manufacturer's instructions (Thermo Fisher). In this protocol, peptides (100 µg) are loaded onto a pH-resistant resin and then desalted with water washing combined with low speed centrifugation. A step-gradient of increasing acetonitrile concentration in a high-pH elution solution is then applied to columns to elute bound peptides into 8 fractions. Following elution, fractions were frozen and lyophilized.

nLC-MS/MS for TMT proteomics

nLC-MS/MS was performed as described previously[36]. Peptide fractions were suspended in 0.1% formic acid at a concentration of 0.25 µg/µL, following peptide quantification (ThermoFisher). All samples were subjected to nanoLC-MS/MS analysis using an UltiMate 3000 RSLCnano system (Thermo Fisher) coupled to a Q Exactive PlusHybrid Quadrupole-Orbitrap mass spectrometer (Thermo Fisher) viaa nanoelectrospray ionization source. For each injection of 4 µL (1 µg), the sample was first trapped on an Acclaim PepMap^{TM}100 20 mm × 0.075 mm trapping column (Thermo Fisher) 5 µl/min at 98/2 v/v

water/acetonitrile with 0.1% formic acid, after which the analytical separation was performed over a 90-min gradient (flow rate of 300 nanoliters/min) of 3 to 30% acetonitrile using a 2 µm EASY-Spray PepMap^{TM}RSLC C18 75 µm × 250 mm column (Thermo Fisher) with a column temperature of 55 °C. MS1 was performed at 70,000 resolution, with an AGC target of 1×10^6 ions and a maximum IT of 60 ms. MS2 spectra were collected by data-dependent acquisition (DDA) of the top 20 most abundant precursor ions with a charge greater than 1 per MS1 scan, with dynamic exclusion enabled for 30s. Precursor ions were filtered with a 1.0 m/z isolation window and fragmented with a normalized collision energy of 30. MS2 scans were performed at 17,500 resolution, AGC target of 1×10^5 ions, and a maximum IT of 60 ms.

Data analysis for TMT proteomics

Proteome Discoverer 2.2 (PDv2.2) was used for raw data analysis, with default search parameters including oxidation (15.995 Da on M) as a variable modification and carbamidomethyl (57.021 Da on C) and TMT6plex (229.163 Da on peptide N-term and K) as fixed modifications, and 2 missed cleavages (full trypsin specificity). Data were searched against human Mito Carta 2.0 database[64]. PSMs were filtered to a 1% FDR. PSMs were grouped to unique peptides while maintaining a 1% FDR at the peptide level. Peptides were grouped to proteins using the rules of strict parsimony and proteins were filtered to 1% FDR using the Protein FDR Validator node of PD2.2. MS2 reporter ion intensities for all PSMs having co-isolation interference below 0.5 (50% of the ion current in the isolation window) and an average S/N > 10 for reporter ions were summed together at the peptide and protein level. Imputation was performed via low abundance resampling.

Statistical analysis for TMT proteomic

The protein group tab in the PDv2.2 results was exported as tab delimited.txt. files, and analyzed based on a previously described workflow[36]. First, M2 reporter (TMT) intensities were summed together for each TMT channel, each channel's sum was divided by the average of all channels' sums, resulting in channel-specific loading control normalization factors to correct for any deviation from equal protein input in the 10-plex experiments. Reporter intensities for proteins were divided by the loading control normalization factors for each respective TMT channel. All loading control-normalized reporter intensities were converted to $\log_2$ space and the average value from the ten samples per kit was subtracted from each sample specific measurement to normalize the relative measurements to the mean of each kit. Data from each kit were then combined for statistical comparisons. For comparison of PBMC to leukemia cell lines, condition average, standard deviation, p-value (p, two-tailed student's t-test, assuming equal variance), and adjusted p-value ($P_{adjusted}$, Benjamini Hochberg FDR correction) were calculated[65,66]. For protein-level quantification, only Master Proteins—or the most statistically significant protein representing a group of parsimonious proteins containing common peptides identified at 1% FDR—were used for quantitative comparison.

Proteomics data availability and software

All raw data for proteomics experiments is available online using accession number “PXD020715” for Proteome Xchange[67] and accession number “JPST000934” for jPOST Repository[68].

Statistical Analysis and Software

Statistical analysis was performed using GraphPad Prism 8.4. Among groups, data were analyzed using one-way ANOVA and Tukey’s multiple comparison tests. The assumption of equal variance was assessed using the Brown-Forsythe test. All data are represented as mean ± SEM and analysis were conducted with a significance level set at $p<0.05$. Details of statistical analysis are included within figure legends. Figures were generated using Biorender and GraphPad Prism 8.4.

Declarations

AKNOWLEDGEMENTS

The work was supported by DOD-W81XWH-19-1-0213 (K.H.F.-W.) and NIH P01 CA171983 (M.C.C). This project used the North Carolina Tissue Consortium (NCTC) shared resource which is supported in part by the University Cancer Research Fund (UCRF).

AUTHOR CONTRIBUTIONS

K.H.F.-W. conceived and designed the study. M.A.N., K.L.M., J.T.H., H.S.C., C.S. and K.H.F.-W performed the experiments. M.A.N, K.L.M., and K.H.F.-W prepared the figures and wrote the manuscript. All authors reviewed and approved the manuscript.

ETHICS DECLARATION

The authors of this manuscript declare no competing interests.

References

1. Fisher-Wellman, K. H. *et al.* Mitochondrial Diagnostics: A multiplexed assay platform for comprehensive assessment of mitochondrial energy fluxes. *Cell Rep.* 3593-3606.e10 (2018).
2. Benador, I. Y. *et al.* Mitochondria Bound to Lipid Droplets Have Unique Bioenergetics, Composition, and Dynamics that Support Lipid Droplet Expansion. *Cell Metab.* (2018) doi:10.1016/j.cmet.2018.03.003.
3. Sullivan, L. B. *et al.* Supporting Aspartate Biosynthesis Is an Essential Function of Respiration in Proliferating Cells. *Cell* **162**, 552–563 (2015).
4. Lechuga-Vieco, A. V. *et al.* Cell identity and nucleo-mitochondrial genetic context modulate OXPHOS performance and determine somatic heteroplasmy dynamics. *Sci. Adv.* (2020) doi:10.1126/sciadv.aba5345.

5. Forner, F., Foster, L. J., Campanaro, S., Valle, G. & Mann, M. Quantitative proteomic comparison of rat mitochondria from muscle, heart, and liver. *Mol. Cell. Proteomics* (2006) doi:10.1074/mcp.M500298-MCP200.
6. Thor Johnson, D. *et al.* Tissue heterogeneity of the mammalian mitochondrial proteome. *Am J Physiol Cell Physiol* (2007) doi:10.1152/ajpcell.00108.2006.—The.
7. Baeza, J., Smallegan, M. J. & Denu, J. M. Mechanisms and Dynamics of Protein Acetylation in Mitochondria. *Trends in Biochemical Sciences* (2016) doi:10.1016/j.tibs.2015.12.006.
8. Grimsrud, P. A. *et al.* A quantitative map of the liver mitochondrial phosphoproteome reveals posttranslational control of ketogenesis. *Cell Metab.* (2012) doi:10.1016/j.cmet.2012.10.004.
9. Škrtić, M. *et al.* Inhibition of Mitochondrial Translation as a Therapeutic Strategy for Human Acute Myeloid Leukemia. *Cancer Cell* **20**, 674–688 (2011).
10. Sriskanthadevan, S. *et al.* AML cells have low spare reserve capacity in their respiratory chain that renders them susceptible to oxidative metabolic stress. *Blood* **125**, 2120–2130 (2015).
11. Suganuma, K. *et al.* Energy metabolism of leukemia cells: Glycolysis versus oxidative phosphorylation. *Leuk. Lymphoma* **51**, 2112–2119 (2010).
12. Goto, M. *et al.* Importance of glutamine metabolism in leukemia cells by energy production through TCA cycle and by redox homeostasis. *Cancer Invest.* **32**, 241–247 (2014).
13. Lee, E. A. *et al.* Targeting mitochondria with avocatin B induces selective leukemia cell death. *Cancer Res.* **75**, 2478–2488 (2015).
14. Kao, L. P. *et al.* Chemotherapy selection pressure alters sphingolipid composition and mitochondrial bioenergetics in resistant HL-60 cells. *J. Lipid Res.* (2019) doi:10.1194/jlr.RA119000251.
15. Goto, M. *et al.* Adaptation of leukemia cells to hypoxic condition through switching the energy metabolism or avoiding the oxidative stress. *BMC Cancer* **14**, 1–9 (2014).
16. Farge, T. *et al.* Chemotherapy-resistant human acute myeloid leukemia cells are not enriched for leukemic stem cells but require oxidative metabolism. *Cancer Discov.* **7**, 716–735 (2017).
17. Kuntz, E. M. *et al.* Targeting mitochondrial oxidative phosphorylation eradicates therapy-resistant chronic myeloid leukemia stem cells. *Nat. Med.* **23**, 1234–1240 (2017).
18. Xiang, W. *et al.* Pyrvinium selectively targets blast phase-chronic myeloid leukemia through inhibition of mitochondrial respiration. *Oncotarget* (2015) doi:10.18632/oncotarget.5615.
19. Panina, S. B., Pei, J., Baran, N., Konopleva, M. & Kirienko, N. V. Utilizing Synergistic Potential of Mitochondria-Targeting Drugs for Leukemia Therapy. *Front. Oncol.* **10**, (2020).
20. Guièze, R. *et al.* Mitochondrial Reprogramming Underlies Resistance to BCL-2 Inhibition in Lymphoid Malignancies. *Cancer Cell* **36**, 369-384.e13 (2019).
21. Dykens, J. A. & Will, Y. The significance of mitochondrial toxicity testing in drug development. *Drug Discovery Today* (2007) doi:10.1016/j.drudis.2007.07.013.
22. Cohen, B. H. Pharmacologic effects on mitochondrial function. *Developmental Disabilities Research Reviews* (2010) doi:10.1002/ddrr.106.

23. Fisher-Wellman, K. H. *et al.* Mitochondrial Diagnostics: A Multiplexed Assay Platform for Comprehensive Assessment of Mitochondrial Energy Fluxes. *Cell Rep.* **Sep 25;24**, 3593–3606 (2018).
24. Fisher-Wellman, K. H. *et al.* Respiratory Phenomics across Multiple Models of Protein Hyperacylation in Cardiac Mitochondria Reveals a Marginal Impact on Bioenergetics. *Cell Rep.* (2019) doi:10.1016/j.celrep.2019.01.057.
25. McLaughlin, K. L., McClung, J. M. & Fisher-Wellman, K. H. Bioenergetic consequences of compromised mitochondrial DNA repair in the mouse heart. *Biochem. Biophys. Res. Commun.* 3–9 (2018) doi:10.1016/j.bbrc.2018.09.022.
26. Martínez-Reyes, I. *et al.* Mitochondrial ubiquinol oxidation is necessary for tumour growth. *Nature* (2020) doi:10.1038/s41586-020-2475-6.
27. Inoue, T., Swain, A., Nakanishi, Y. & Sugiyama, D. Multicolor analysis of cell surface marker of human leukemia cell lines using flow cytometry. in *Anticancer Research* (2014).
28. Mrózek, K., Tanner, S. M., Heinonen, K. & Bloomfield, C. D. Molecular cytogenetic characterization of the KG-1 and KG-1a acute myeloid leukemia cell lines by use of spectral karyotyping and fluorescence in situ hybridization. *Genes Chromosom. Cancer* **38**, 249–252 (2003).
29. Rücker, F. G. *et al.* Molecular profiling reveals myeloid leukemia cell lines to be faithful model systems characterized by distinct genomic aberrations. *Leukemia* (2006) doi:10.1038/sj.leu.2404235.
30. Jitschin, R. *et al.* Mitochondrial metabolism contributes to oxidative stress and reveals therapeutic targets in chronic lymphocytic leukemia. *Blood* **123**, 2663–2672 (2014).
31. Veech, R. L., Kashiwaya, Y., Gates, D. N., King, M. T. & Clarke, K. The energetics of ion distribution: The origin of the resting electric potential of cells. *IUBMB Life* **54**, 241–252 (2002).
32. Luptak, I. *et al.* Decreased ATP production and myocardial contractile reserve in metabolic heart disease. *J. Mol. Cell. Cardiol.* **116**, 106–114 (2018).
33. Roth, K. & Weiner, M. W. Determination of cytosolic ADP and AMP concentrations and the free energy of ATP hydrolysis in human muscle and brain tissues with 31P NMR spectroscopy. *Magn. Reson. Med.* (1991) doi:10.1002/mrm.1910220258.
34. Glancy, B., Willis, W. T., Chess, D. J. & Balaban, R. S. Effect of calcium on the oxidative phosphorylation cascade in skeletal muscle mitochondria. *Biochemistry* **52**, 2793–2809 (2013).
35. Messer, J. I., Jackman, M. R. & Willis, W. T. Pyruvate and citric acid cycle carbon requirements in isolated skeletal muscle mitochondria. *Am. J. Physiol. Cell Physiol.* **286**, C565-572 (2004).
36. McLaughlin, K. L., Kew, K. A., McClung, J. M. & Fisher-Wellman, K. H. Subcellular proteomics combined with bioenergetic phenotyping reveals protein biomarkers of respiratory insufficiency in the setting of proofreading-deficient mitochondrial polymerase. *Sci. Rep.* (2020) doi:10.1038/s41598-020-60536-y.
37. Ryu, I. *et al.* L-Deprenyl exerts cytotoxicity towards acute myeloid leukemia through inhibition of mitochondrial respiration. *Oncol. Rep.* **40**, 3869–3878 (2018).

38. Rai, Y., Yadav, P., Kumari, N., Kalra, N. & Bhatt, A. N. Hexokinase II inhibition by 3-bromopyruvate sensitizes myeloid leukemic cells K-562 to anti-leukemic drug, daunorubicin. *Biosci. Rep.* (2019) doi:10.1042/bsr20190880.
39. Lee, D. *et al.* Folate cycle enzyme MTHFD1L confers metabolic advantages in hepatocellular carcinoma. *J. Clin. Invest.* (2017) doi:10.1172/JCI90253.
40. Singh, R. P. *et al.* Disrupting Mitochondrial Copper Distribution Inhibits Leukemic Stem Cell Self-Renewal. *Cell Stem Cell* **26**, 926-937.e10 (2020).
41. Chevrollier, A., Loiseau, D., Reynier, P. & Stepien, G. Adenine nucleotide translocase 2 is a key mitochondrial protein in cancer metabolism. *Biochim. Biophys. Acta - Bioenerg.* **1807**, 562–567 (2011).
42. Maldonado, E. N. *et al.* ATP/ADP turnover and import of glycolytic ATP into mitochondria in cancer cells is independent of the adenine nucleotide translocator. *J. Biol. Chem.* **291**, 19642–19650 (2016).
43. Sanchez-Martin, C. *et al.* Honokiol Bis-Dichloroacetate Is a Selective Allosteric Inhibitor of the Mitochondrial Chaperone TRAP1. *Antioxid. Redox Signal.* **00**, 1–13 (2020).
44. Sanchez-Martin, C. *et al.* Rational Design of Allosteric and Selective Inhibitors of the Molecular Chaperone TRAP1. *Cell Rep.* **31**, 107531 (2020).
45. Kim, D. *et al.* Development of pyrazolo[3,4-d]pyrimidine-6-amine-based TRAP1 inhibitors that demonstrate in vivo anticancer activity in mouse xenograft models. *Bioorg. Chem.* **101**, 103901 (2020).
46. Li, X. T., Li, Y. S., Shi, Z. Y. & Guo, X. L. New insights into molecular chaperone TRAP1 as a feasible target for future cancer treatments. *Life Sci.* **254**, 117737 (2020).
47. Yoshida, S. *et al.* Molecular chaperone TRAP1 regulates a metabolic switch between mitochondrial respiration and aerobic glycolysis. *Proc. Natl. Acad. Sci. U. S. A.* **110**, (2013).
48. Sciacovelli, M. *et al.* The mitochondrial chaperone TRAP1 promotes neoplastic growth by inhibiting succinate dehydrogenase. *Cell Metab.* **17**, 988–999 (2013).
49. Bryant, K. G. *et al.* A Mitochondrial-targeted purine-based HSP90 antagonist for leukemia therapy. *Oncotarget* (2017) doi:10.18632/oncotarget.23097.
50. Ramkumar, B., Dharaskar, S. P., Mounika, G., Paithankar, K. & Sreedhar, A. S. Mitochondrial chaperone, TRAP1 as a potential pharmacological target to combat cancer metabolism. *Mitochondrion* **50**, 42–50 (2020).
51. Kamal, A. *et al.* A high-affinity conformation of Hsp90 confers tumour selectivity on Hsp90 inhibitors. *Nature* **425**, 407–410 (2003).
52. Willis, W. T., Jackman, M. R., Messer, J. I., Kuzmiak-Glancy, S. & Glancy, B. A simple hydraulic analog model of oxidative phosphorylation. *Med. Sci. Sports Exerc.* (2016) doi:10.1249/MSS.0000000000000884.
53. Jitschin, R. *et al.* Mitochondrial metabolism contributes to oxidative stress and reveals therapeutic targets in chronic lymphocytic leukemia. *Blood* (2014) doi:10.1182/blood-2013-10-532200.

54. Byrd, J. C. *et al.* Targeting BTK with ibrutinib in relapsed chronic lymphocytic leukemia. *N. Engl. J. Med.* (2013) doi:10.1056/NEJMoa1215637.
55. Chevrollier, A., Loiseau, D., Reynier, P. & Stepien, G. Adenine nucleotide translocase 2 is a key mitochondrial protein in cancer metabolism. *Biochimica et Biophysica Acta - Bioenergetics* (2011) doi:10.1016/j.bbabio.2010.10.008.
56. Lee, C. H. *et al.* Adenine Nucleotide Translocase 2 as an Enzyme Related to [18F] FDG Accumulation in Various Cancers. *Mol. Imaging Biol.* **21**, 722–730 (2019).
57. Krycer, J. R. *et al.* Dynamic Metabolomics Reveals that Insulin Primes the Adipocyte for Glucose Metabolism. *Cell Rep.* (2017) doi:10.1016/j.celrep.2017.11.085.
58. Thompson, C. B. & Bielska, A. A. Growth Factors Stimulate Anabolic Metabolism by Directing Nutrient Uptake. *J. Biol. Chem.* jbc.AW119.008146 (2019) doi:10.1074/jbc.aw119.008146.
59. Buck, M. D. D. *et al.* Mitochondrial Dynamics Controls T Cell Fate through Metabolic Programming. *Cell* (2016) doi:10.1016/j.cell.2016.05.035.
60. Vardhana, S. A. *et al.* Impaired mitochondrial oxidative phosphorylation limits the self-renewal of T cells exposed to persistent antigen. *Nat. Immunol.* (2020) doi:10.1038/s41590-020-0725-2.
61. Ryan, T. E. *et al.* Extensive skeletal muscle cell mitochondriopathy distinguishes critical limb ischemia patients from claudicants. *JCI insight* (2018) doi:10.1172/jci.insight.123235.
62. Ivanusic, D., Madela, K. & Denner, J. Easy and cost-effective stable positioning of suspension cells during live-cell imaging. *J. Biol. Methods* **4**, 80 (2017).
63. Schindelin, J. *et al.* Fiji: An open-source platform for biological-image analysis. *Nature Methods* (2012) doi:10.1038/nmeth.2019.
64. Calvo, S. E., Clauser, K. R. & Mootha, V. K. MitoCarta2.0: An updated inventory of mammalian mitochondrial proteins. *Nucleic Acids Res.* (2016) doi:10.1093/nar/gkv1003.
65. Naugler, C. & Lesack, K. An open-source software program for performing Bonferroni and related corrections for multiple comparisons. *J. Pathol. Inform.* (2011) doi:10.4103/2153-3539.91130.
66. Benjamini, Y. & Hochberg, Y. Controlling the false discovery rate: a practical and powerful approach to multiple testing. *J. R. Stat. Soc. Ser. B* (1995) doi:10.2307/2346101.
67. Deutsch, E. W. *et al.* The ProteomeXchange consortium in 2017: Supporting the cultural change in proteomics public data deposition. *Nucleic Acids Res.* (2017) doi:10.1093/nar/gkw936.
68. Okuda, S. *et al.* JPOSTrepo: An international standard data repository for proteomes. *Nucleic Acids Res.* (2017) doi:10.1093/nar/gkw1080.

Figures

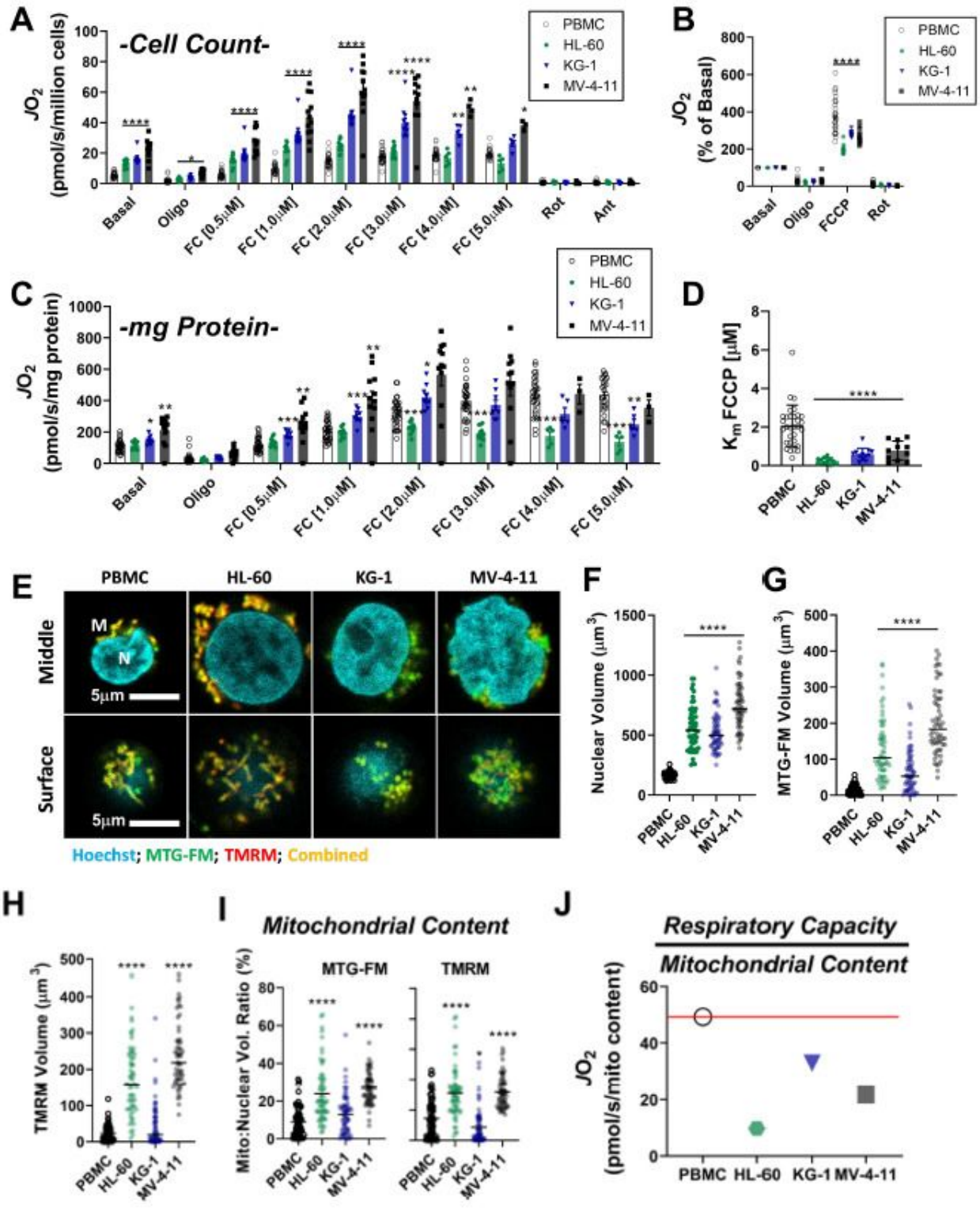

Figure 1

Leukemia exhibit impaired cellular respiratory capacity amid an increased mitochondrial network All experiments were performed in intact cells. FCCP-stimulated flux normalized to cell count (A) and protein concentration (C) and represented as percentage of basal respiration (B). (D) Km of FCCP calculated from FCCP titration (cell lines n=12, PBMC n=31). (E-I) Confocal microscopy was performed using two mitochondrial targeted cationic fluorescent dyes, MitoTracker Green FM (MTG-FM) and TMRM. (E)

Representative fluorescent images of nuclear volume (F) and mitochondrial volume as measured by MTG-FM (G) and TMRM labelling (H) (n=65 cells/cell type). (I) Ratios of mitochondrial to nuclear volumes assessed by MTG-FM and TMRM labelling. (J) Respiratory deficiency of cell type calculated by comparing respiratory capacity (the protein-normalized maximal respiration rate) to mitochondrial content (mitochondrial TMRM volume). Data are presented as mean ±SEM and analyzed by two-way ANOVA (A-D) and one-way ANOVA (F-I). *p<0.05, **p<0.005, ***p<0.0005, ****p<0.0001.

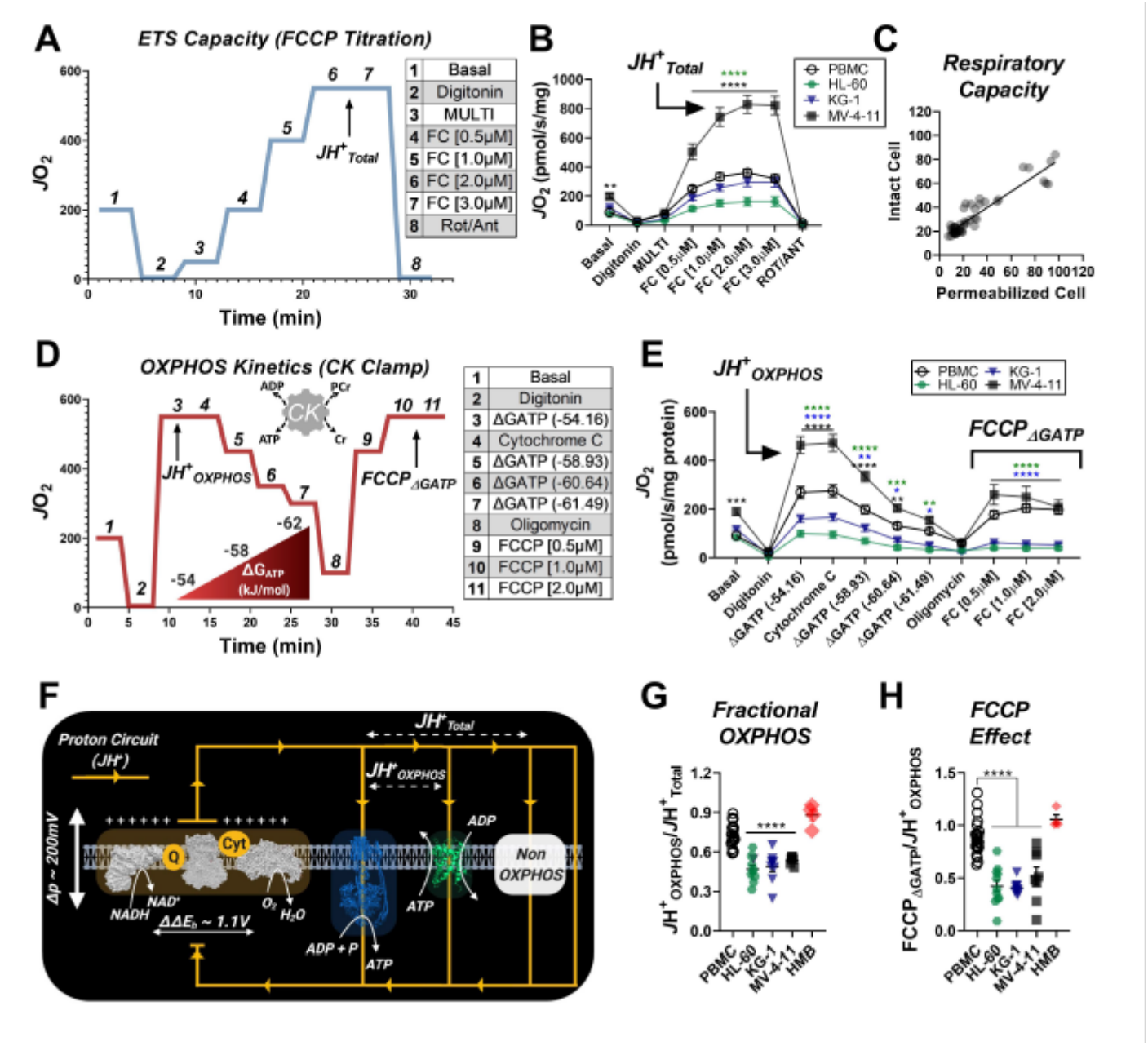

Figure 2

Impaired OXPHOS kinetics and ATP-dependent inhibition of ETS flux are unique phenotypes of leukemic mitochondria All experiments were performed using digitonin-permeabilized cells. (A) Schematic depicting changes in oxygen consumption (JO2) during an ETS capacity protocol (FCCP titration) where points 6-7 represent the maximum proton conductance of the respiratory system (JH+Total). (B) ETS capacity protocol measured in leukemia cell lines and PBMC. (C) Comparison of respiratory capacity

between intact and permeabilized experimental conditions across cell types. (D) Schematic depicting JO2 during an OXPHOS kinetics protocol (ΔGATP titration) where point 3 represents maximum proton conductance by the OXPHOS system (JH+OXPHOS) and point 10-11 represents maximum proton conductance of the respiratory system in the presence of ΔGATP (FCCP ΔGATP). (E) OXPHOS capacity protocol measured in leukemia cell lines and PBMC. (F) Illustration detailing maximal proton current generated by the electron transport system (JH+Total) and proportion of current harnessed by the phosphorylation system (JH+OXPHOS). (G) Comparison of fractional OXPHOS calculated as the ratio of JH+OXPHOS to JH+Total. (H) Comparison of FCCP effect calculated as the ratio of FCCP ΔGATP to JH+OXPHOS. For all experiments, n=10 for leukemia cell lines and n=22 for PBMC. Data are presented as mean ±SEM and analyzed by two-way ANOVA in (B,E) and one-way ANOVA in (G,H). *p<0.05, **p<0.005, ***p<0.0005, ****p<0.0001.

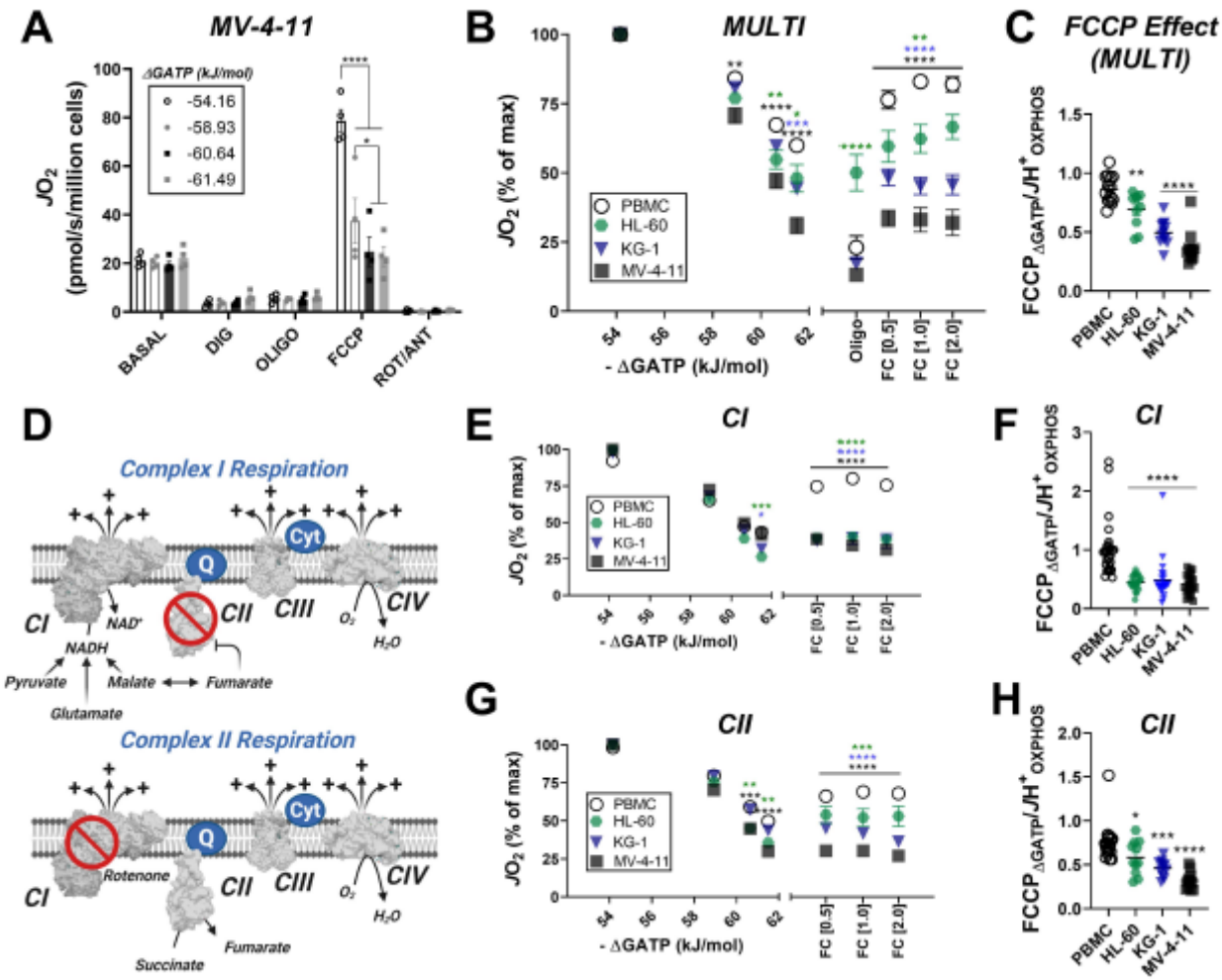

Figure 3

In leukemic mitochondria ΔGATP regulates ETS flux independent of substrate condition (A) FCCP-stimulated flux was measured under four ATP-free energy (ΔGATP) conditions in permeabilized MV-4-11 cells. n=4 independent experiments. (B) OXPHOS kinetics supported by MULTI (Pyr/M/G/S/Oct) substrate condition in mitochondria isolated from PBMC and leukemia cells. (C) Comparison of FCCP effect

calculated as the ratio of FCCP ΔGATP to JH+OXPHOS from B. (D) Schematic depicting CI supported respiration driven by pyruvate/glutamate/malate and inhibition of CII by equilibration of malate/fumarate (top) and CII supported respiration driven by succinate and inhibition of CI by rotenone (bottom). OXPHOS kinetics of mitochondria isolated from PBMC and leukemia cells and supported by Complex I substrates (E) and Complex II substrates (G). FCCP effect of complex I (F) and complex II (H) supported respiration. n=7-10 for leukemia cell lines and n=22 for PBMC. Data are mean ±SEM and analyzed by one-way ANOVA in (A) and two-way ANOVA in (B-C, E-H). *p<0.05, **p<0.005, ***p<0.0005, ****p<0.0001.

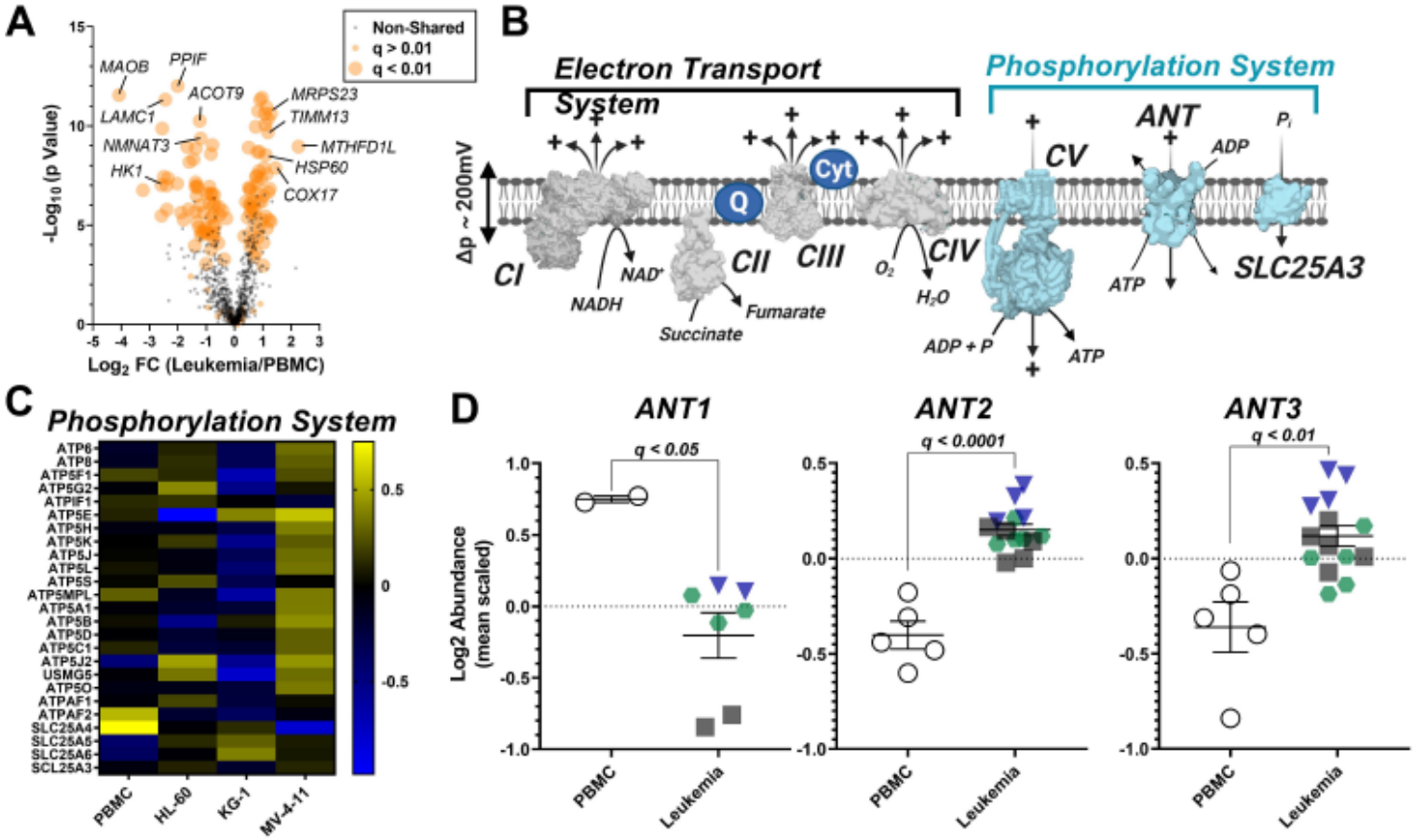

Figure 4

Analysis of mitochondrial proteome reveal disparate expression of ANT isoforms in leukemia TMT-labelled nLC-MS/MS was performed on mitochondrial lysates from each cell type. (A) Volcano plot depicting changes in proteome between leukemia cell lines and PBMC with mitochondrial proteins shown in orange. Significance in abundance is indicated by size of each circle with changes in significance (p<0.01) represented by larger circles. (B) Schematic depicting the OXPHOS system with enzymes integral to the ETS shown in gray and the phosphorylation system shown in blue. (C) Heat map displaying the common differentially expressed proteins across the phosphorylation system of leukemia and PBMC cells. Data are displayed as Log2 protein intensity of all quantified master proteins. (D) Comparison of log2 abundance of ANT isoforms in leukemia and PBMC. n=4-6 mitochondrial preparations per cell lines. Data are presented as mean ±SEM and analyzed by unpaired t-tests.

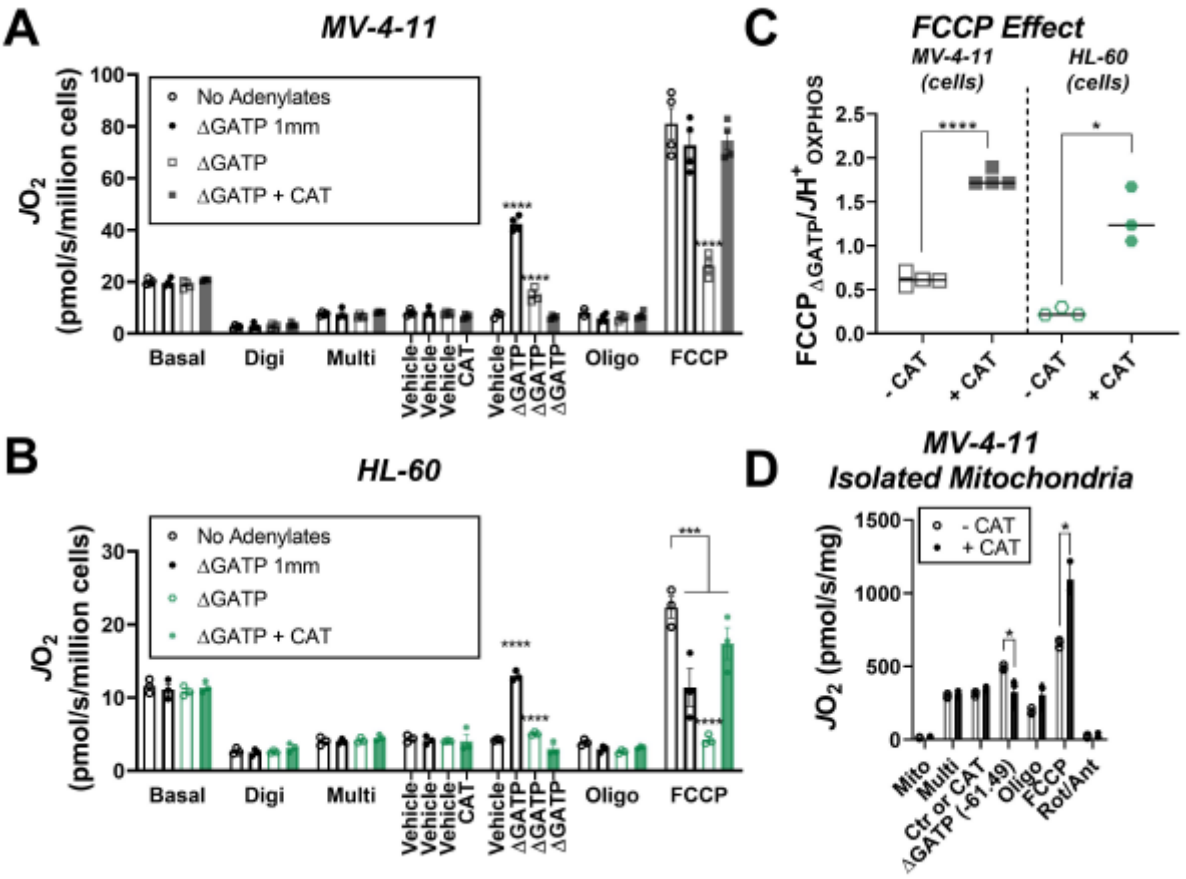

Figure 5

Inhibition of ETS flux by ΔGATP requires ANT (A,B) OXPHOS kinetics was performed in the absence of adenylates or in the presence of low ΔGATP (-54.16), high ΔGATP (-61.49), or high ΔGATP + CAT (Carboxyatractyloside; ANT inhibitor). Comparison of OXPHOS kinetics in MV-4-11 (A) and HL-60 cells (B). (C) Ratio of FCCP ΔGATP to JH+OXPHOS with and without CAT in MV-4-11 and HL-60 cells. (D) OXPHOS kinetics measured in the presence of CAT in mitochondria isolated from MV-4-11. n=4 independent experiments per cell type. Data are presented as mean ±SEM and analyzed by two-way ANOVA (A-B), paired t-tests (C) and unpaired t-tests (D). *p<0.05, ***p<0.0005, ****p<0.0001

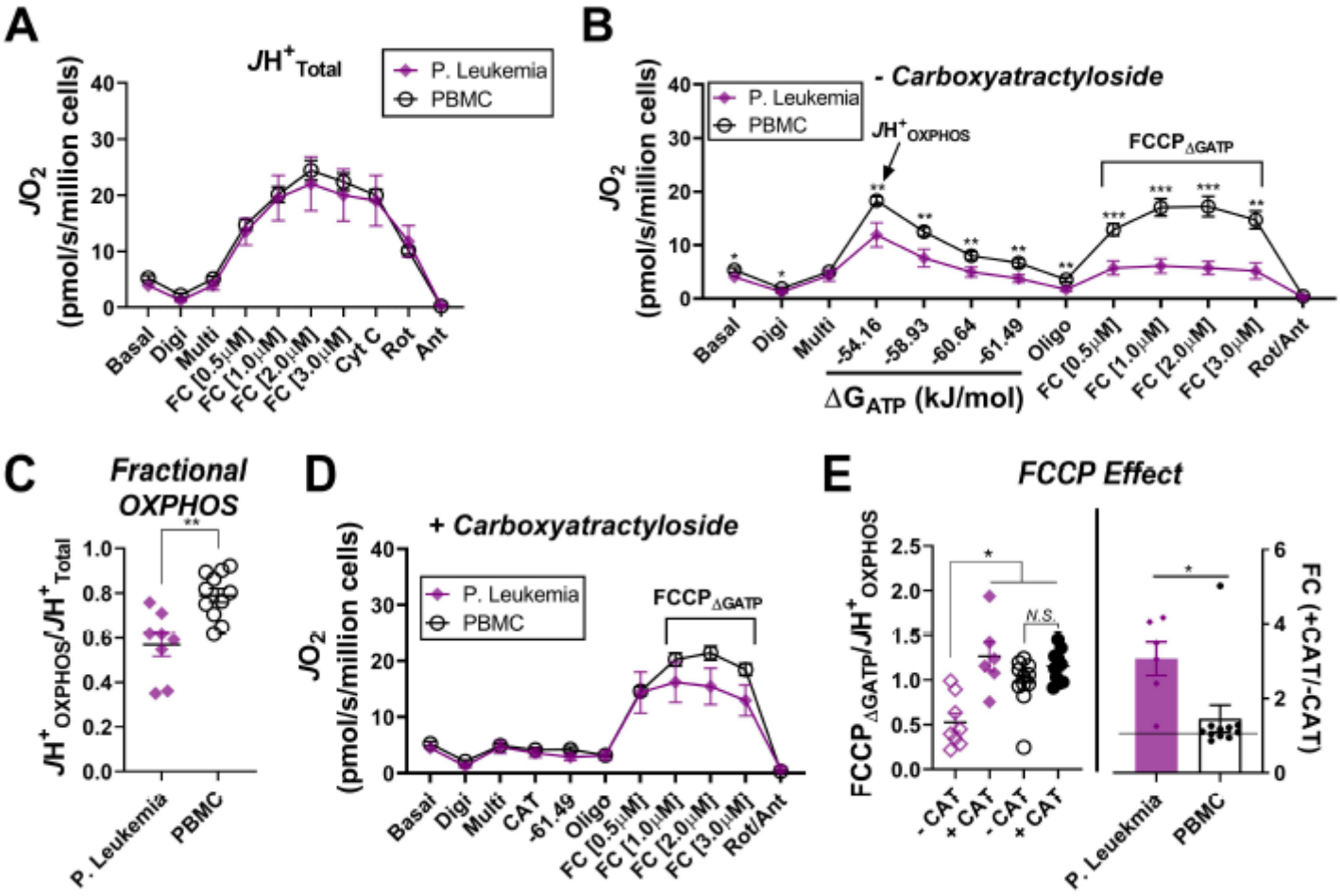

Figure 6

Bioenergetic efficiency is reduced in human primary leukemia Permeabilized cells were used for all experiments. JO2 of primary leukemia and PBMC were measured by ETS capacity (A) and OXPHOS kinetic (B) protocols. (C) Comparison of fractional OXPHOS in primary leukemia and PBMC. (D) Comparison of OXPHOS kinetics in the presence of CAT. Primary leukemia n=8, PBMC n=11 (E) Ratio of FCCP ΔGATP to JH+OXPHOS with and without CAT in primary leukemia and PBMC (left) and calculated fold change (right). Data are presented as mean ±SEM and analyzed by unpaired t-tests (A-D, E;right) and paired t-tests (E;left). *p<0.05, **p<0.005, ***p<0.0005

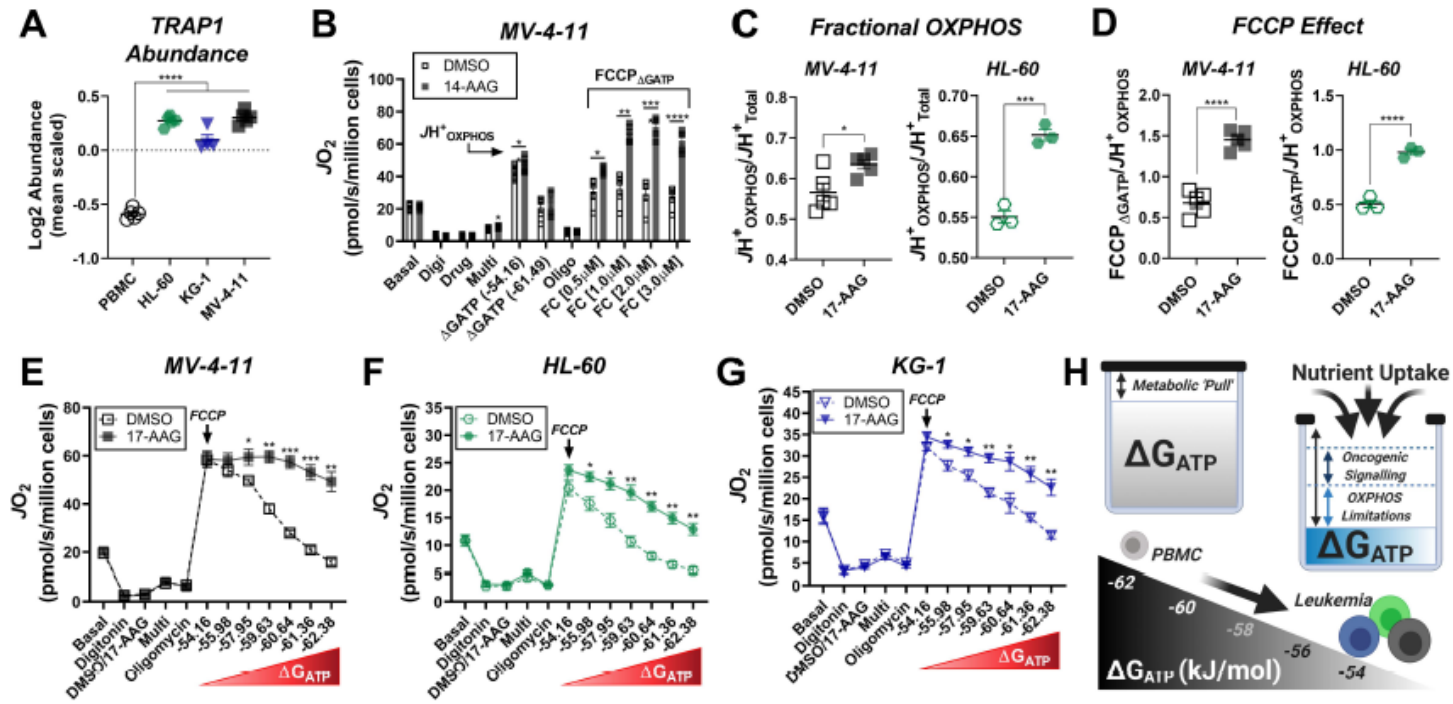

Figure 7

Inhibition of ETS flux by ΔGATP is regulated by TRAP1 (A) Log2 Abundance of TRAP1 in PBMC and leukemia cells, n=6 per cell line. (B) Comparison of OXPHOS kinetics in presence of the TRAP1 inhibitor, 17-AAG. N=7 independent cell experiments. Comparison of (C) fractional OXPHOS and (D) FCCP effect in MV-4-11 and HL-60 cells in presence of 17-AAG. N=3 independent experiments/cell line. (E-G) Comparison of respiratory flux inhibition within leukemia cell lines across a range of ΔGATP induced by functional TRAP1. Respiration was stimulated by the additional FCCP (1µM). (G) Schematic depicting low ΔGATP and chronically accelerated nutrient uptake in leukemia, driven by oncogenic signaling and intrinsic OXPHOS limitations. Data are presented as mean ±SEM and analyzed by unpaired t-tests (A-E). *p<0.05, **p<0.005, ***p<0.0005, ****p<0.0001

Supplementary Files

This is a list of supplementary files associated with this preprint. Click to download.

- SupplementalFigures.pdf
- SupplementaryTable1.xlsx